Characterization of the nanostructures of a lithographically patterned dot array by x-ray pseudo-Kossel lines

D. R. Lee,[a] Y. S. Chu, Y. Choi,[b] J. C. Lang, and G. Srajer
Advanced Photon Source, Argonne National Laboratory, Argonne, Illinois 60439

S. K. Sinha
Department of Physics, University of California, San Diego, La Jolla, California 92093 and Los Alamos National Laboratory, Los Alamos, New Mexico 87545

V. Metlushko
Department of Electrical and Computer Engineering, University of Illinois at Chicago, Chicago, Illinois 60607

B. Ilic
School of Applied and Engineering Physics, Cornell University, Ithaca, New York 14853

(Received 4 November 2002; accepted 9 December 2002)

Grazing x-ray scattering from a nanofabricated periodic dot array exhibits an interesting diffraction pattern, resembling x-ray Kossel lines, due to the anisotropic x-ray resolution function. We demonstrate that the unique diffraction pattern can be used for precise characterization of the deep nanostructures, which cannot be obtained accurately by microscopy techniques. © *2003 American Institute of Physics.* [DOI: 10.1063/1.1543249]

Periodic arrays of nanostructured dots have attracted much attention during the last decade because of their potential as future high-density optical and magnetic storage media. The unique properties of these nanosystems depend strongly on their structural parameters, such as size, shape, and array spacing,[1–3] which have become controllable owing to recent advances in nanofabrication technology. Various scanning probe microscopies, such as scanning electron microscopy (SEM) and atomic force microscopy (AFM) have been employed for the topographical metrology of the dot arrays. However, as the aspect ratio of height to width for the nanoarrays increases, accurate characterization of the ''deep'' nanostructures becomes increasingly challenging due to technical problems, such as the tip-sample convolution in AFM.[4] X-ray scattering, without such intrinsic limitations, can be effectively used to characterize the structural details of deep nanostructures. In addition, it offers the additional advantage of measuring the buried interfaces, if needed. However, quantitative analysis of a typical x-ray diffraction pattern from a nanofabricated two-dimensional (2D) dot array ($0.1\sim1\ \mu$m period) requires careful consideration of the resolution function of the probe,[5] because its reciprocal space density is many orders of magnitude higher than those of typical solid-state or biological crystals. Consequently, the measured diffraction pattern exhibits characteristic features[5] due to the highly anisotropic nature of the instrumental resolution function, which can be understood as analogs of Kossel lines[6] (or *pseudo*-Kossel lines). In this letter, we explain the origin of such pseudo-Kossel lines and then demonstrate how these features can be used for precise structural characterization of 2D nanodot arrays.

For this study, a square array of circular disk-shaped dots with a period of 750 nm and a diameter of 340 nm was fabricated using a standard lithography and lift-off process.[7] The required pattern was written in a single poly(methylmethacrylate) layer with e-beam lithography, and a Gd film of nominal thickness of 50 nm was deposited using e-beam evaporation. An area of 0.5×0.5 mm^2 was patterned on a 10×10 mm^2 Si/SiO_2 wafer. X-ray diffraction measurements were performed using a 9-keV ($\lambda=1.3776$ Å) monochromatic x-rays at the SRI-CAT beamlines 1-BM, 2-BM, and 4-ID-D, at the Advanced Photon Source. The incident beam with its angular divergence of 1 mrad (horizontal) and 0.05 mrad (vertical) was used. The diffracted beam was collected by a scintillation detector with 1-mrad (horizontal) and 0.1-mrad (vertical) acceptance. We define a coordinate system such that the $x-z$-plane coincides with the vertical scattering plane, and the z-axis is perpendicular to the sample surface. As depicted in the insets of Fig. 1, the azimuth angle ϕ measures the rotation of the reciprocal axes q_x and q_y with respect to x- and y-axes about the z-axis. Since the measurements presented here were made at a fixed q_z value of 0.18 Å^{-1}, a point in the reciprocal space is indexed using only two indices (H,K), using the relationship $q_x=(2\pi/a)H$ and $q_y=(2\pi/a)K$, where a is the period of the nanoarray. Consequently, a radial ($q_r=\sqrt{q_x^2+q_y^2}$) scan through a reciprocal point (H,K) was carried out by performing a theta rocking scan at $\phi=\tan^{-1}(K/H)$. Since the patterned area is much smaller than the total area of the substrate, the diffuse scattering from the substrate surface was subtracted using the dynamical expression in Ref. 8 [see the dashed lines in Figs. 1(a) and 1(b)], and the diffraction intensities from the dot array were then obtained, as shown in Fig. 2.

The mathematical diffraction pattern constructed from a 2D square dot array consists of one-dimensional (1D) rods along the q_z direction, going through (H,K) integer points. Thus, a 2D diffraction pattern at a fixed q_z value corresponds to a set of discrete intensities at (H,K) integer points. Experimentally, however, a typical q_r scan along (HK) direc-

[a]Electronic mail: drlee@aps.anl.gov
[b]Also at: Department of Materials Science and Engineering, Northwestern University, Evanston, IL 60208.

 © 2003 American Institute of Physics
Downloaded 24 Jun 2003 to 164.54.56.3. Redistribution subject to AIP license or copyright, see http://ojps.aip.org/aplo/aplcr.jsp

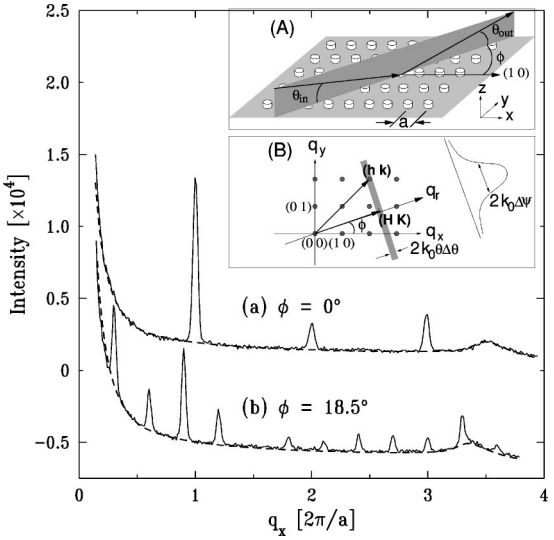

FIG. 1. Radial scans measured along (a) (1 0) [$\phi=0°$] and (b) (3 1) [$\phi=18.5°$] directions from a Gd dot array. Dashed lines represent the calculated diffuse scattering intensities from the substrate surface. Insets (A) and (B) show schematics of the scattering geometry and its corresponding diffraction configuration in the reciprocal plane. The gray stripe represents the resolution volumes when scanning along q_r.

tion yields a number of peaks at noninteger positions, with the exception of that along the (1 0) direction. For example, a q_r scan along the (3 1) direction produces noninteger peaks at $(3n/10,n/10)$, as shown in Fig. 2. In fact, these noninteger peaks are not points but are the cross sections of streaks, which will be discussed subsequently. We attribute the observed diffraction pattern to the resolution function, which describes the broadening of the reciprocal resolution of the probe primarily due to the divergence of the incident beam and the finite acceptance of the detector. The resolution function projected onto the q_x-q_y plane can be described as an ellipse with its minor and major axes parallel and perpendicular to the q_r-direction. The lengths of the minor and major axes are, $k_0\Delta\psi$ and $k_0\theta\Delta\theta$, respectively, where $\Delta\psi$ and $\Delta\theta$ are effective horizontal and vertical angular broadenings, respectively.[9] The grazing incident geometry ($\theta \ll 1$) and our experimental setup with smaller vertical divergence and detector acceptance make the elliptical sampling area virtually a stripe with the length-to-width ratio of a few hundreds, as illustrated in Fig. 1(inset B). Consequently, the measurement performed at an arbitrary point, $\mathbf{G}_0=(H,K)$, picks up the intensities from the neighboring diffraction rods $\mathbf{G}=(h,k)$ within the sampling area. A simple condition, in which $\mathbf{G}_0$, $\mathbf{G}$, and $(\mathbf{G}-\mathbf{G}_0)$ forms a right triangle, can be expressed as

$$hH+kK=H^2+K^2. \tag{1}$$

A simple rearrangement of Eq. (1) gives the following set of equations for circle with a radius r_{hk}, which collectively produces the observed 2D diffraction pattern in Fig. 3(a),

$$\left(H-\frac{h}{2}\right)^2+\left(K-\frac{k}{2}\right)^2=\left(\frac{h}{2}\right)^2+\left(\frac{k}{2}\right)^2=r_{hk}^2. \tag{2}$$

For example, the solid circle overlaying on the data in Fig. 3(a) corresponds to $(h,k)=(2,2)$. The observed diffraction pattern with a set of circles is an analog of well-known Kossel lines from the radiation excited in the crystal sample, which is widely used in the most precise determinations of lattice constants.[6] Thus, we refer to these as *pseudo*-Kossel lines. Interestingly, the origin of the diffraction patterns discussed here bears a striking resemblance to the origin of diffraction patterns from quasicrystals, which can also be regarded as the projection from a higher-dimensional reciprocal lattice onto a lower-dimensional space.[10] Our case corresponds to the projection of a 2D lattice into a 1D subspace. Similarly to the real Kossel lines for the crystalline samples,

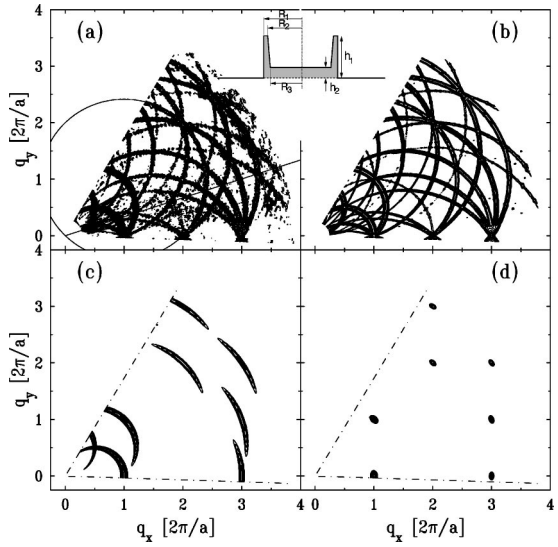

FIG. 3. Contour map of intensity distribution in the q_x-q_y reciprocal plane: (a) measurements; (b), (c), and (d) calculations with horizontal resolution widths of 2.75×10^{-3} Å^{-1}, 2.75×10^{-4} Å^{-1}, and 2.75×10^{-5} Å^{-1}, respectively. For reference, $2\pi/a$ corresponds to 8.37×10^{-4} Å^{-1}. The circle in (a) shows a pseudo-Kossel circle satisfying Eq. (2), and the line represents the trajectory of a radial scan along the (3 1) direction in Fig. 1(b). Weak intensities at (2,0) and (2,1) in (d) result from destructive interferences due to the ratio between the array period and dot radius. The inset shows a cross-sectional drawing of the model used for the best fit.

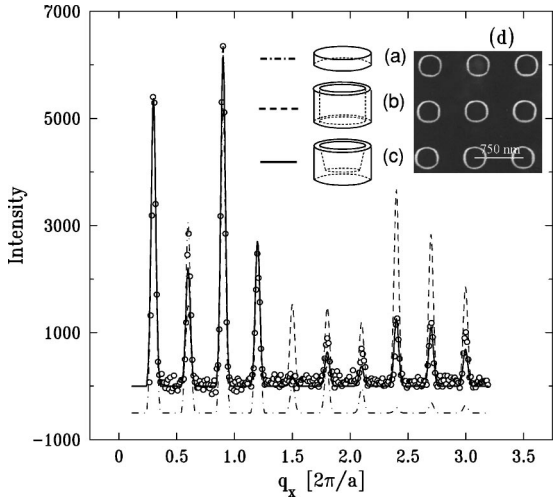

FIG. 2. Diffraction intensities of the radial scan along the (3 1) direction ($\phi=18.5°$) after subtracting diffuse scattering intensities from the substrate surface. Circles represent measurements, and lines represent the calculations with different models: (a) circular disks (dash-dot line), (b) ring cylinders (dashed line), and (c) crowns (solid). For clarity, the dash-dot line is shifted. Inset (d) shows a SEM picture from the sample.

Downloaded 24 Jun 2003 to 164.54.56.3. Redistribution subject to AIP license or copyright, see http://ojps.aip.org/aplo/aplcr.jsp

the pseudo-Kossel lines can be used for precise characterization of the nanostructures of the dot array as described subsequently.

The diffracted intensity I at (H,K) can be expressed in the Born approximation as

$$I(H,K)=|F(q_z)|^2\sum_{h,k}|F(h,k)|^2\mathcal{R}(H,K;h,k), \tag{3}$$

where the weight function, $\mathcal{R}(H,K;h,k)=\exp\{-[1/2(k_0\Delta\psi)^2][(h-H)^2+(k-K)^2](4\pi^2/a^2)\}$, accounts for the lengthwise Gaussian profile of the resolution stripe. $F(q_z)$ is the 1D form factor along q_z direction, and $F(h,k)$ is the 2D form factor on the q_x-q_y plane. For a disk-shaped dot with a radius R, $F(h,k)$ is given simply by $2\pi R^2(J_1(q_rR)/q_rR)$, where J_1 is the first-order Bessel function and $q_r=(2\pi/a)\sqrt{h^2+k^2}$.[11] However, as shown in Fig. 2, this simple model (the dash-dot line) cannot explain the experimental data (circles) measured along the (3 1) direction, and, therefore, a more realistic model should be taken into account.

As seen from the SEM image in Fig. 2(d), dots are not a simple disk, but rather have the thin ''crown'' on the top due to the photoresist removal process,[12] as illustrated in Fig. 2(c). This finding was also confirmed by our AFM measurements, although the exact profile of the crown could not be measured. The form factor $F(h,k)$ of crown dots can be then written as

$$\begin{aligned}F(h,k)&=2\pi h_2\int_0^{R_3}rJ_0(q_rr)dr+2\pi\int_{R_3}^{R_2}[\alpha r+(h_2\\&\quad-\alpha R_3)]rJ_0(q_rr)dr+2\pi h_1\int_{R_2}^{R_1}rJ_0(q_rr)dr\\&=\frac{2\pi h_1R_1}{q_r}J_1(q_rR_1)+\frac{2\pi\alpha}{q_r^2}\Big[R_2J_0(q_rR_2)\\&\quad-R_3J_0(q_rR_3)-\int_{R_3}^{R_2}J_0(q_rr)dr\Big],\end{aligned} \tag{4}$$

where $\alpha=(h_1-h_2)/(R_2-R_3)$, J_0 is the zeroth order Bessel function, and $R_{1,2,3}$ and $h_{1,2}$ are radii and heights of crown dots, respectively, as depicted in the inset of Fig. 3. In this approximation, the height profile of the crown is modeled as an effective density profile of a disk. This treatment can be justified because the 2D form factor is sensitive only to the projected electronic density on the $x-y$ plane. The solid line in Fig. 2 represents the diffracted intensities calculated for this crown model using Eqs. (3) and (4), and shows good agreement with measurements. On the other hand, the dashed line calculated from a model of simple rings, as depicted in Fig. 2(b), overestimated the intensities at high q_r values. From the best fit, for which only six parameters were adjusted, R_1, (R_1-R_2), and (R_3-R_2) were estimated to be 170 ± 15, 22 ± 4, and 18 ± 5 nm, respectively, and the ratio h_1/h_2 was 4 ± 0.8. The horizontal and vertical resolution widths for the best fit were used as $2.75(\pm0.50)\times10^{-3}$ Å^{-1} and $1.76(\pm0.04)\times10^{-5}$ Å^{-1}, respectively, in good agreement with the experimental condition, mentioned earlier. Therefore, the broadening due to the long-range disorder of the dots, as mentioned in Ref. 5, can be neglected in our study.

Using the fitted parameters describing the average nanostructures of the dot array, we simulated the 2D diffraction pattern on the q_x-q_y plane, which excellently reproduces the measured 2D diffraction pattern [see Figs. 3(a) and 3(b)]. To check the sensitivity of the pseudo-Kossel lines, we compared the best fit with the simulations calculated using the effective horizontal resolutions of 2.75×10^{-4} Å^{-1} [Fig. 3(c)] and 2.75×10^{-5} Å^{-1} [Fig. 3(d)], but with the same vertical resolution. It should be mentioned that these horizontal (out-of-scattering-plane) resolutions correspond to angular broadenings of 60 and 6 μrad, respectively, which can be hardly obtained in the typical scattering experiments. In our model, the effect due to the limited transverse coherence length of the incident x-rays, in comparison with the period of the dot array, is not explicitly treated, but rather absorbed in the description of the effective broadening of the resolution function. Such distinction is difficult to make without employing a detector with a high spatial resolution.[13]

In summary, we have demonstrated that the diffraction pattern from the nanofabricated dot array originates from the highly anisotropic instrumental resolution function in the grazing diffraction geometry. In addition, these pseudo-Kossel lines can provide precise structural characterization on the periodic nanofabricated patterns, which are difficult to ascertain using microscopy techniques.

We thank D. J. Kim for the AFM measurements. Work at Argonne is supported by the U.S. DOE, Office of Basic Energy Sciences, under Contract No. W-31-109-ENG-38. One of the authors (V.M.) is supported by the U.S. NSF, Grant No. ECS-0202780. Another author (S.K.S.) is supported by the U.S. DOE, BES-DMS, under contract No. W-7405-ENG-36.

[1] R. P. Cowburn, D. K. Koltsov, A. O. Adeyeye, M. E. Welland, and D. M. Tricker, Phys. Rev. Lett. **83**, 1042 (1999).
[2] J. A. Johnson, M. Grimsditch, V. Metlushko, P. Vavassori, B. Ilic, P. Neuzil, and R. Kumar, Appl. Phys. Lett. **77**, 4410 (2000).
[3] J. Rothman, M. Kläui, L. Lopez-Diaz, C. A. F. Vaz, A. Bleloch, J. A. C. Bland, Z. Cui, and R. Speaks, Phys. Rev. Lett. **86**, 1098 (2001).
[4] K. Wilder, C. F. Quate, B. Singh, R. Alvis, and W. H. Arnold, J. Vac. Sci. Technol. B **14**, 4004 (1996); M. F. Tabet and F. K. Urban III, *ibid.* **15**, 800 (1997).
[5] D. Rafaja, V. Valvoda, J. Kub, K. Temst, M. J. Van Bael, and Y. Bruynseraede, Phys. Rev. B **61**, 16144 (2000).
[6] W. Kossel, V. Loeck, and H. Voges, Z. Phys. **94**, 139 (1935); J. M. Cowley, *Diffraction Physics* (Elsevier, Amsterdam, 1995), Chap. 14; V. P. Glazkov, A. V. Irodova, V. A. Somenkov, and S. Sh. Shil'shteĭn, JETP Lett. **44**, 216 (1986).
[7] V. Metlushko, U. Welp, G. W. Crabtree, Z. Zhang, S. R. J. Brueck, B. Watkins, L. E. DeLong, B. Ilic, K. Chung, and P. J. Hesketh, Phys. Rev. B **59**, 603 (1999).
[8] S. K. Sinha, E. B. Sirota, S. Garoff, and H. B. Stanley, Phys. Rev. B **38**, 2297 (1988).
[9] A. Braslau, P. S. Pershan, G. Swislow, B. M. Ocko, and J. Als-Nielsen, Phys. Rev. A **38**, 2457 (1988).
[10] V. Elser, Phys. Rev. B **32**, 4892 (1985); A. I. Goldman and K. F. Kelton, Rev. Mod. Phys. **65**, 213 (1993).
[11] B. P. Toperverg, G. P. Felcher, V. V. Metlushko, V. Leiner, R. Siebrecht, and O. Nikonov, Physica B **283**, 149 (2000).
[12] F. Rousseaux, D. Decanini, F. Carcenac, E. Cambril, M. F. Ravet, C. Chappert, N. Bardou, B. Bartenlian, and P. Veillet, J. Vac. Sci. Technol. B **13**, 2787 (1995).
[13] A. Gibaud, J. Wang, M. Tolan, G. Vignaud, and S. K. Sinha, J. Phys. I **6**, 1085 (1996).

Downloaded 24 Jun 2003 to 164.54.56.3. Redistribution subject to AIP license or copyright, see http://ojps.aip.org/aplo/aplcr.jsp